Journal of Hazardous Materials 162 (2009) 1355–1363

Contents lists available at ScienceDirect

Journal of Hazardous Materials

journal homepage: www.elsevier.com/locate/jhazmat

Removal of basic dye by modified Unye bentonite, Turkey

Erdal Eren*

Department of Chemistry, Ahi Evran University, Faculty of Arts and Science, 40100 Kırşehir, Turkey

ARTICLE INFO

Article history:
Received 3 December 2007
Received in revised form 6 June 2008
Accepted 9 June 2008
Available online 13 June 2008

Keywords:
Dye adsorption
Clay
Kinetic
Surface charge
X-ray diffraction

ABSTRACT

The adsorption behavior of crystal violet (CV^+) from aqueous solution onto raw (RB) and manganese oxide-modified (MMB) bentonite samples was investigated as a function of parameters such as initial CV^+ concentration, contact time and temperature. The Langmuir, Freundlich and Dubinin–Radushkevich (D–R) adsorption models were applied to describe the equilibrium isotherms. The Langmuir monolayer adsorption capacities of RB and MMB were estimated as 0.32 and 1.12 mmol/g, respectively. The mean adsorption energy derived from D–R isotherm for MMB showed that the type of adsorption of dye molecules on this material may be defined as chemical adsorption. The adsorption rate was fast and more than half of the adsorbed-CV^+ was removed in the first 55 min for RB and 5 min for MMB at the room temperature. The pseudo-first-order, pseudo-second-order kinetic and the intraparticle diffusion models were used to describe the kinetic data and rate constants were evaluated. The thermodynamic parameters such as ΔH, ΔS and ΔG were found 117.41 kJ/mol, 41.50 J/(mol K), −5.07 kJ/mol (RB) and 21.19 kJ/mol 98.34 J/(mol K), −7.84 kJ/mol (MMB) at 295.15 K, respectively. The quite high adsorption capacity and high adsorption rate of MMB will provide an important advantage for using of this material in basic dye solution.

1. Introduction

Dyes are widely used in industries such as textiles, leather, printing, food, plastics, etc. The removal of dyes from industrial wastewaters is a major problem. Conventional methods for the removal of dyes from wastewater include adsorption onto solid substrates, chemical coagulation, oxidation, filtration and biological treatment. Adsorption is one of the effective separation technique to remove dilute pollutants as well as offering the potential for regeneration, recovery and recycling of the adsorbend material [1]. The study of dye adsorption onto a cost-effective adsorbent is significant in the industrial wastewater treatment system because it provides valuable insights into the mechanisms and the optimum operation parameters of adsorption processes. Bentonite has been proven to be a promising material for the removal of contaminants from wastewater. Not only bentonite is abundant, but also it is really an efficient and economic adsorbent for adsorption of pollutants including dyes, oil, and heavy-metals. It belongs to the 2:1 clay family, which mainly consists of montmorillonite, the basic structural unit of which is composed of two tetrahedrally coordinated sheets of silicon ions surrounding a sandwiched octahedrally coordinated sheet of aluminum ions. The isomorphous substitution of Al^{3+} for Si^{4+} in the tetrahedral layer and Mg^{2+} for Al^{3+} in the octahedral layer results in a net negative surface charge on the clay. Compared with other types of clays, it has excellent adsorption properties and possesses adsorption sites available within its interlayer space as well as on the outer surface and edges [2].

Bentonite is widely applied in many fields of adsorption technology including the removal of metals [3,4], phenols [5–7], organic molecules [8,9], polymers [10,11], pesticides [12], radionuclides [13], and dyes [14,15]. A composite adsorbent, manganese oxide-modified bentonite (MMB), was proposed and studied in this research. The reason for choosing manganese oxides is that relative to Fe or Al oxides, manganese oxides have a higher affinity for cations. In fact, several investigators have suggested applications for manganese oxides in water and wastewater treatment [16–20]. Bentonite, which has a high surface area, should provide an efficient surface for the manganese oxide. At the same time, the manganese oxides can improve the large organic cation adsorption capacity of bentonite.

The present study is planned to assess the effectiveness of the manganese oxide-modified bentonite sample in the removal of large organic cation from aqueous solutions. In order to elucidate the role of bentonite surface in the crystal violet (CV^+) adsorption process, the influence of pH, ionic strength and temperature on the adsorption of crystal violet (CV^+) by the RB and MMB samples was investigated to better understand the large organic cation adsorption process.

* Tel.: +90 386 211 45 25.
E-mail address: eeren@ahievran.edu.tr.

0304-3894/$ – see front matter © 2008 Elsevier B.V. All rights reserved.
doi:10.1016/j.jhazmat.2008.06.016

Nomenclature

C_e	equilibrium concentration of the adsorbate in the solution (mmol/L)
CV^+	crystal violet
D_p	average pore diameter
k_1	pseudo-first-order rate constant of sorption ($1h^{-1}$)
k_2	pseudo-second-order rate constant of sorption (g/(mmol min))
k_i	constant of intraparticle diffusion (g/(mmol $min^{1/2}$))
K_L	constant that represents the energy or net enthalpy of adsorption (L/g)
K_F	Freundlich constant indicative of the adsorption capacity of the adsorbent (mmol/g)
m	mass of adsorbent (g/L)
MMB	manganese oxide-modified bentonite
n	experimental constant indicative of the adsorption intensity of the adsorbent
q_e	amount of adsorbate removed from aqueous solution at equilibrium (mmol/g)
q_t	amount of adsorbate sorbed on the sorbent surface at any time t (mmol/g)
q_m	mass of adsorbed solute completely required to saturate a unit mass of adsorbent (mmol/g)
RB	raw bentonite
S_{BET}	the BET surface area
$S_{ext.}$	external surface area (including only mesopores)
$S_{mic.}$	micropores surface area
t	reaction time (min)
V_t	total pore volume

2. Experimental

2.1. Materials

2.1.1. Preparation of RB

The bentonite sample (from Unye, Turkey) was ground and washed in deionized water several times at a 1:10 bentonite/water ratio. The mixture was stirred for 3 h and then kept standing overnight, followed by seperation, washing and drying at 60 °C. RB had a mineral composition of 76% montmorillonite, 8% quartz, 12% dolomite and 4% other minerals. Whitness is found to be 85%. RB was composed of 62.70% SiO_2, 20.10% Al_2O_3, 2.16% Fe_2O_3, 2.29% CaO, 3.64% MgO, 0.27% Na_2O, 2.53% K_2O, 0.21% TiO_2, and 0.02% P_2O_5. The ignition loss of the RB at 1273 K was also found to be 6.1%. The cation exchange capacity (CEC), determined with triethanolamine-buffered $BaCl_2$ solution (c = 0.1 M) followed by a re-exchange with aqueous $MgCl_2$ solution (c = 0.1 M), is of 0.65 mmol/g [21], and the major exchangeable cations are: Ca (57.1%), Mg (28.8%), Na (10.5%) and K (3.8%). The total pore volume value is 0.07 cm^3/g, the micropores contribute to 11.42% of total pore volume. The average pore diameter is 8.11 nm (Table 1).

2.1.2. Preparation of MMB

Manganese chloride and sodium hydroxide were mainly used in the modification of RB to enhance the adsorption capacity of RB. 20 g of RB were immersed in sufficient 2.0 M sodium hydroxide for 4 h and temperature of the reaction mixture was maintained at 90 °C. The RB was dispersed into 150 mL of 0.1 M $MnCl_2$ aqueous solution. 300 mL of 0.1 M NaOH aqueous solution was added slowly with a drop rate 1 mL/h. The titration was carried out under nitrogen flow throughout the procedure to minimize unexpected reactions, e.g. formation of carbonate salts. The obtained powder was rinsed with 0.01 M HCl aqueous solution to remove the excess $Mn(OH)_2$ precipitated on the outer surface of the clay and further washed with deionized water. The oxidation was performed in aqueous suspension system at room temperature. The $Mn(OH)_2$ intercalated compound prepared as above was dispersed in 50 mL of 1.5 M H_2O_2 basic solution and vigorously stirred. The color of the sample immediately turned from original light color to dark brown, indicating the oxidation of the hydroxide into oxide phase. For equilibrium, the suspension was further stirred for 24 h. The powder sample was washed with deionized water and dried at 60 °C [22].

2.2. Dye adsorption measurement

Adsorption of CV^+ (C.I. No. 42555, dye content, ~90%, chloride salt, obtained from Reidel-de Haen) was carried out by a batch technique to obtain equilibrium data. CV^+ was not purified prior to use. Equilibrium adsorption isotherms of dye were undertaken at 295.15 K. For isotherm studies, adsorption experiments were carried out by adding 50 mg of the bentonite sample to 50 mL of CV^+ solution of varying concentration, in a series of 100 mL polyethylene flasks. Each polyethylene flask was filled with 50 mL aqueous solution of CV^+ and adjusted to desired pH (2.5–8.5), ionic strength (0–0.6 M), and temperature (295.15–309.15 K). The pH values were adjusted by adding a few drops of dilute NaOH or HCl, and were measured by a Jenway 3040 model pH-meter, and the pH-meter was calibrated using buffer solutions of pH 4.0 and 9.0 before use. The suspensions were centrifuged at 5000 rpm at the end of the adsorption process. The concentration of the dye in the solution was analyzed spectrophotometrically using a Unicam UV2-100 Spectrophotometer. The measurements were made at the wavelength λ = 590 nm, which corresponds to maximum absorbance. Blanks containing no dye were used for each series of experiments. All the experiments were carried out in duplicate.

2.3. Characterization methods

The mineralogical compositions of the RB and MMB samples were determined from the X-ray diffraction (XRD) patterns of the products taken on a Rigaku 2000 automated diffractometer using Ni filtered Cu Kα radiation. XRD analysis of the bentonite was performed using the three-principal lines [23]. A Tri Star 3000 (Micromeritics, USA) surface analyzer was used to measure nitrogen adsorption isotherm at 77 K in the range of relative pressure 10^{-6} to 1. Before measurement, the sample was degassed at 300 °C for 2 h. The surface areas were calculated by the BET (Brunauer–Emmett–Teller) method. The BET surface area (S_{BET}),

Table 1
Porous structure parameters of the RB and MMB samples

Sample	S_{BET} (m^2/g)	$S_{ext.}$ [a] (m^2/g)	$S_{mic.}$ (m^2/g)	V_t (cm^3/g)	$V_{mic.}$ (cm^3/g)	$V_{meso.}$ (cm^3/g)	D_p [b] (nm)
RB	36.17	19.86	16.30	0.07	0.008	0.067	8.11
MMB	63.70	36.80	26.90	0.08	0.013	0.067	5.30

[a] $S_{ext.} = S_{meso.}$
[b] 4 V/A by BET.

external surface area (including only mesopores $S_{ext.}$), micropores surface area ($S_{mic.}$), total pore volume (V_t) and average pore diameter (D_p) results obtained by applying the BET equation to N_2 adsorption at 77 K and Barret–Joymer–Halenda (BJH) equation to N_2 adsorption at 77 K are listed in Table 1.

3. Results and discussion

3.1. Data processing

The adsorption capacity of CV^+ molecules adsorbed per gram adsorbent (mg/g) was calculated using the equation:

$$q_e = \frac{(C_0 - C_e)V}{m} \quad (1)$$

where q_e the equilibrium concentration of CV^+ on the adsorbent (mmol/g), C_0 the initial concentration of the CV^+ solution (mmol/L), C_e the equilibrium concentration of the CV^+ solution (mmol/L), m the mass of adsorbent (g), and V the volume of CV^+ solution (L).

The adsorption isotherm indicates how the adsorption molecules distribute between the liquid phase and the solid phase when the adsorption process reaches an equilibrium state. The analysis of the isotherm data by fitting them to different isotherm models is an important step to find the suitable model that can be used for design purpose. There are several isotherm equations available for analyzing experimental adsorption equilibrium data. In this study, the equilibrium experimental data for adsorbed CV^+ on bentonite sample were analyzed using the Langmuir and Freundlich models. These isotherms are as follows:

(a) Langmuir isotherm model [24]:

$$\frac{C_e}{q_e} = \frac{C_e}{q_m} + \frac{1}{K_L q_m} \quad (2)$$

where C_e is equilibrium concentration of CV^+ (mmol/L) and q_e is the amount of the CV^+ adsorbed (mmol) by per unit of bentonite (g). q_m and K_L are the Langmuir constants related to the adsorption capacity (mmol/g) and the equilibrium constant (L/g), respectively.

(b) Freundlich isotherm model [25]:

$$\log\ q_e = \log K_F + \left(\frac{1}{n}\right) \log C_e \quad (3)$$

where K_F and n are Freundlich constants related to adsorption capacity and adsorption intensity, respectively.

The equilibrium data were also applied to the Dubinin–Radushkevich (D–R) isotherm model to determine if adsorption occurred by physical or chemical processes. The linearized form of the D–R isotherm [26–28] is as follows:

$$\ln\ q_e = \ln q_m - \beta\varepsilon^2 \quad (4)$$

where β is the activity coefficient related to mean adsorption energy (mol^2/J^2) and ε is the Polanyi potential ($\varepsilon = RT \ln(1 + (1/C_e))$. The D–R isotherm is applied to the data obtained from the empirical studies.

The mean adsorption energy, E (kJ/mol) is as follows:

$$E = \frac{1}{\sqrt{-2\beta}} \quad (5)$$

The thermodynamic parameters of the adsorption process were determined from the experimental data using the following equations:

$$\ln\ K_d = \frac{\Delta S}{R} - \frac{\Delta H}{RT} \quad (6)$$

$$\Delta G = \Delta H - T\ \Delta S \quad (7)$$

$$K_d = \frac{q_e}{C_e} \quad (8)$$

where K_d is the distribution coefficient, ΔS, ΔH and ΔG are the changes of entropy, enthalpy and the Gibbs free energy, T (K) is the temperature, R (J/(mol K)) is the gas constant, C_e (mmol/L) and q_e (mmol/L) are the equilibrium concentration in aqueous phase and the amount of CV^+ adsorbed per unit mass of the adsorbent, respectively.

Several kinetic models are available to understand the behavior of the adsorbent and also to examine the controlling mechanism of the adsorption process and to test the experimental data. In the present investigation, the adsorption data were analyzed using three kinetic models, the pseudo-first-order, pseudo-second-order kinetics and the intraparticle diffusion models.

The first order model was presented by Lagergren [29]. The Lagergren's first-order reaction model is expressed as follows:

$$\log(q_e - q_t) = \log\ q_e - \left(\frac{k_1}{2.303}\right) t \quad (9)$$

where q_e and q_t are the amounts of dye (mmol/g) adsorbed on the clay at equilibrium, and at time t, respectively and k_1 is the rate constant (min^{-1}). The rate constant, k_1 was obtained from slope of the linear plots of $\log(q_e - q_t)$ against t.

The adsorption data was also analyzed in terms of pseudo-second-order mechanism, described by Ho and McKay [30]

$$\frac{t}{q_t} = \left(\frac{1}{h}\right) + \left(\frac{1}{q_e}\right) t \quad (10)$$

and the initial rate of adsorption h is

$$h = k_2 {q_e}^2 \quad (11)$$

where k_2 is the rate constant of pseudo-second-order adsorption (g/(mmol min)), h is the initial rate of adsorption (mmol/(g min)). If pseudo-second-order kinetics is applicable, the plot of t/q_t against t of Eq. (11) should give a linear relationship from which the constants q_e, h and k_2 can be determined.

In adsorption systems where there is the possibility of intraparticle diffusion being the rate-limiting step, the intraparticle diffusion approach described by Weber and Morris [31] is used. This equation can be described as (Eq. (12)):

$$q_t = k_d t^{1/2} + c \quad (12)$$

where q_t is the amount of dye adsorbed (mg/g) at time t, k_d (mg/g $min^{1/2}$) is the rate constant for intraparticle diffusion, and c is the intercept.

3.2. Material characterization

The XRD patterns of RB and MMB samples were presented in Fig. 1. For the XRD pattern of RB, one reflection was observed in the region $2^\circ < 2\theta < 8^\circ$ (Fig. 1a). This corresponds to the 5.76° (2θ) value from which the interlamellar distance was found to be 15.33 Å. The XRD results also show that manganese oxide modification has caused structural changes in the MMB. The position of d_{001} peak of MMB sample shifted from 15.33 to 12.41 Å (Fig. 1b). The formation of a new structure was illustrated by the peak appearing at 44.13 Å ($2\theta = 5.12^\circ$) in the XRD pattern of the MMB. This new peak situated at lower 2θ value was likely to appear because of agglomeration of the MMB sheets [32]. Modification has affected mainly the 0 0 1 reflection; the intensities of the 0 2 0, 0 0 6 and 0 6 0 reflections have been increased significantly by the manganese oxide modification process (Table 2). MMB sample displays an increase of the background in the interval between 20° and 30°. The d_{003} reflection of RB at 5.05 Å ($2\theta = 17.52^\circ$) disappeared after modification process. The XRD pattern of the MMB indicated that the MnO_2 saturation caused changing in unit cell dimensions as well as the Bragg angles for several reflections. The results prove that MnO_2 locates in one or

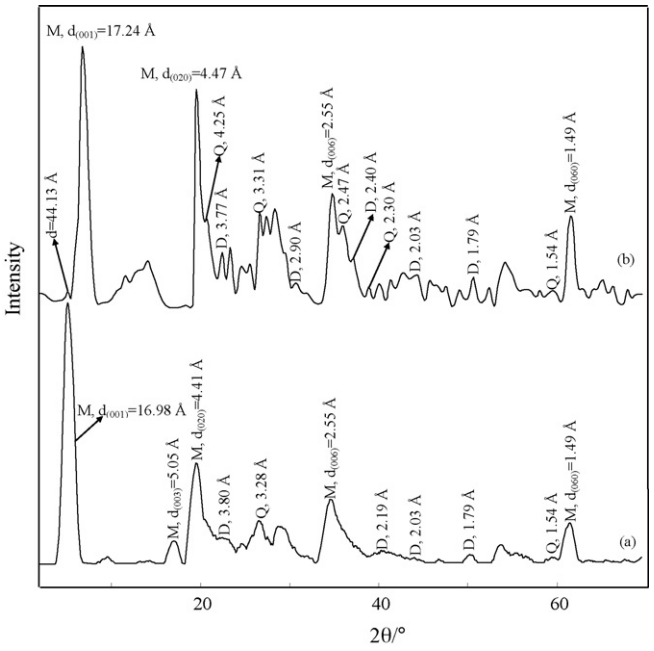

Fig. 1. The X-ray diffraction patterns of the RB (a) and MMB (b) samples (M: montmorillonite).

more types of equivalent positions [33]. The diffractogram of MMB was broader and less intense as compared to RB, suggesting a poorly crystalline structure (Fig. 1 and Table 2).

To better understand surface properties, potentiometric titrations were conducted. Fig. 2 shows proton adsorption curves performed at 0.1 M NaCl supporting electrolyte concentration for the RB and MMB samples. The MMB sample behaved similiarly to MnO_2 where the point of zero charge (pH_{PZC}) of MMB (3.5) was approximately equilvalent to that of MnO_2 (2.4) [34]. However, the pH_{PZC} of RB was approximately 6.8. The pH_{PZC} of MMB falls between the RB and MnO_2. The results suggest that manganese oxides modification process play important role in surface charge behavior of the adsorbent.

3.3. *Effect of solution pH and ionic strength on the CV^+ adsorption*

The adsorption capacities of the bentonite samples towards the CV^+ were determined using various initial solution pH values in the range 3.0–11.0. As shown in Fig. 3, it was observed that the adsorption capacity of RB was nearly independent of pH, while that onto MMB increased with increasing solution pH in the range 3.0–11.0. The lower amount of adsorption in acidic solution is due to the protonation of the surface groups on MMB. Thus, electrostatic repulsion exists between the positively charged surface and the positively charged dye molecule.

Table 2
d-Spacing and intensity values of reflections for bentonite samples

Reflection	RB		MMB	
	d (Å)	Intensity	*d* (Å)	Intensity
d_{001}	15.33	100	12.40	100
d_{003}	5.05	8	–	–
d_{020}	4.42	34	4.47	95
d_{101}	–	–	–	–
d_{006}	2.55	21	2.55	45
d_{060}	1.49	13	1.49	34

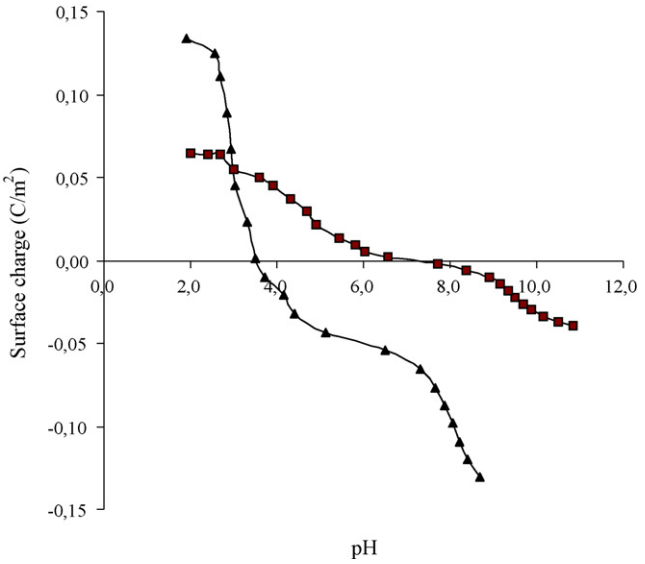

Fig. 2. Surface charge (C/m^2) vs. pH curves of bentonite samples in 0.1 M NaCl solution, squares, RB; triangles, MMB.

The ionic strength of the solution is one of the factors that controls both electrostatic and non-electrostatic interactions between the adsorbate and the adsorbent surface [16]. Fig. 4 shows the equilibrium isotherms for the adsorption of CV^+ on bentonite samples, at different NaCl concentrations (in the range 0.1 and 0.8 M) at pH 6.5. Under these conditions only modified bentonite will be charged negatively inducing the attractive forces between the CV^+ cation and the MMB surface. For MMB the pH_{PZC} is much lower than the pH at which the adsorption process is carried out (3.4 vs. 6.5). When salt is not added, strong attractive forces arise between the CV^+ cation and the MMB. With increasing the ionic strength of the solution a marked decrease in the extent of the adsorption is observed (Fig. 4). This might be explained by the screening effect of added salt resulting in the reduction of the electrostatic attractive interactions. This phenomenon can be attributed to increasing Na^+ concentration with increasing ionic strength and therefore increasing competition for the adsorption sites on the MMB. For RB the attractive forces are very weak because the pH_{PZC} for RB is very close to solution pH (6.8 vs. 6.5). It can be observed that using salt

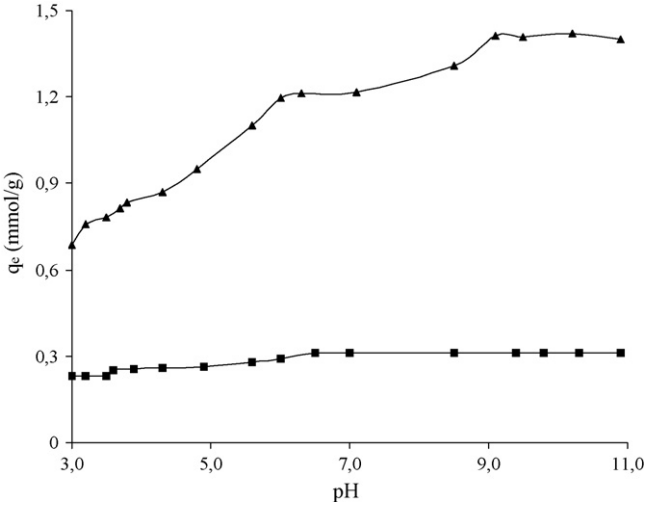

Fig. 3. Effect of pH on adsorption of CV^+ onto bentonite samples, RB, squares; MMB, triangles. Contact time 4 h, T = 295.15 K, C_0 = 1.5 mmol/L, and m = 2 g/L.

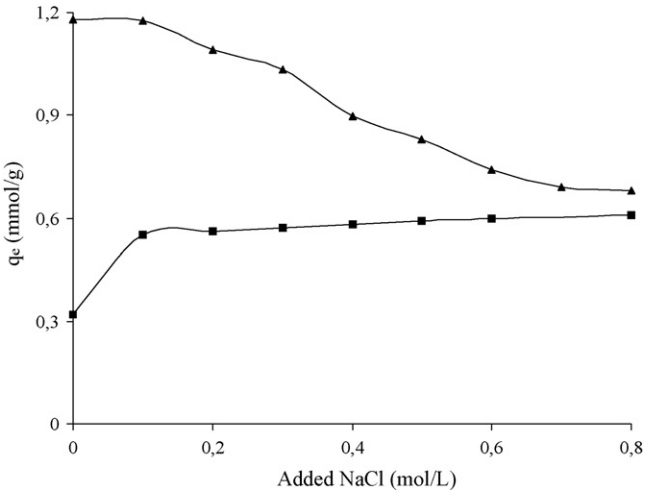

Fig. 4. Effect of ionic strength on adsorption of CV^+ onto bentonite samples, RB, squares; MMB, triangles. Contact time 4 h, T = 295.15 K, C_0 = 1.5 mmol/L, and m = 2 g/L.

concentration of 0.8 M the amount of adsorption is nearly on the same level when 0.1 M is added. This suggests that at pH 6.5 the adsorption of CV^+ on RB is mainly governed by non-electrostatic forces. The extent of the adsorption is determined in this case by the volume of pores accessible to CV^+ cation. Also, the lower CV^+ adsorption in pure water indicates that the bentonite particles are suspended and do not agglomerate, but higher CV^+ adsorption in the presence of electrolyte indicate that the ionic strength of the medium favor the aggregate formation of the RB particles [35], and thus the CV^+ molecules can be entrapped by newly generated centers [36].

3.4. Equilibrium isotherm models

The equilibrium data for CV^+ adsorption on bentonite samples were fitted to Langmuir equation (Eq. (2)): an equilibrium model able to identify chemical mechanism involved. Linear plots of C_e/q_e vs. C_e (not shown) were employed to determine the value of q_m (mg/g) and K_L (L/mg). The data obtained with the correlation coefficients (R^2) was listed in Table 3. The Langmuir monolayer adsorption capacity (q_m) gives the amount of the metal required to occupy all the available sites per unit mass of the sample. The Langmuir monolayer adsorption capacities of RB and MMB were estimated as 0.32 and 1.12 mmol/g, respectively (Table 3). The lower K_L value for the RB (1.61) compared to that for MMB (5.59) indicate that the surface modification process influences the adsorption equilibrium. The high-energy sites with high equilibrium constant (K_L for the MMB) had a significantly higher affinity than that for low-energy sites with low equilibrium constant (K_L for the RB). The high-energy sites on which CV^+ was held had a high adsorption maximum (q_m = 1.12 mmol/g), accounting for ≈350% of total CV^+ adsorption on RB. The low-energy sites on which the dye were loosely held had a low adsorption maximum (q_m = 0.32 mmol/g).

The equilibrium data also fitted to Freundlich equation (Eq. (3)), a fairly satisfactory empirical isotherm can be used for non-ideal adsorption. The Freundlich isotherm constants K_F and n are constants incorporating all factors affecting the adsorption process such as of adsorption capacity and intensity of adsorption. The constants K_F and n were calculated from Eq. (3) and Freundlich plots (not shown). The values for Freundlich constants and correlation coefficients (R^2) for the different adsorbents used during the study are also presented in Table 3. Freundlich parameters (K_F and n) indicate whether the nature of adsorption is either favorable or unfavorable. The intercept is an indicator of adsorption capacity and the slope is an indicator of adsorption intensity. The Freundlich adsorption capacity (K_F) was found to be 0.83 and 1.11 for the RB and MMB samples, respectively. The high value of the intercept, K_F, indicates the high adsorption capacity of MMB. A relatively slight slope $n \ll 1$ indicates that adsorption intensity is favorable over the entire range of concentrations studied, while a steep slope ($n > 1$) means that adsorption intensity is favorable at high concentrations but much less at lower concentrations. In the adsorption systems, n values are 3.58 and 14.92 which indicate that adsorption intensity is favorable over the entire range of concentrations studied.

D–R isotherm constants, q_m, for RB and MMB were found to be 1.12 and 0.42 mmol/g, respectively (Table 3). The adsorption capacity derived from D–R isotherm for RB is nearly equal compared to Langmuir isotherm. This adsorption potential is independent of the temperature, but it varies depending on the nature of adsorbent and adsorbate. The magnitude of E is used for estimating the type of adsorption mechanism. The constants obtained for D–R isotherms are shown in Table 3. The mean adsorption energy (E) gives information about ion-exchange, chemical and physical adsorption. The magnitude of E is useful for estimating the type of adsorption reaction, i.e., an energy range from about 8 to 16 kJ/mol indicates ion-exchange processes [26]. In the case of $E < 8$ kJ/mol weak physical forces, such as van der Waals and hydrogen bonding may affect the adsorption mechanism [26]. In the case of $E > 16$ kJ/mol the type of adsorption may be defined as chemical adsorption [27,28]. The E value of CV^+ adsorption by RB was found to be 11.47 kJ/mol and this implies that the type of adsorption is ion-exchange mechanism [26]. It was found to be 19.55 kJ/mol for MMB. The type of adsorption of CV^+ on the MMB may be defined as chemical adsorption [27,28].

3.5. Thermodynamic parameters

The values of ΔH and ΔS were determined from the slopes and intercepts of the plots of $\ln K_d$ vs. $1/T$ (not shown). As given in Table 4, the adsorption of the CV^+ onto bentonite samples is an endothermic process, which indicates that the amount of the adsorbed dye increases at higher temperatures. This may be attributed to the increased penetration of the CV^+ inside micropores at higher temperatures due to the swelling effect within the internal structure of the bentonite with increasing temperature [37]. The positive values of ΔH also indicate the presence of an energy barrier in the adsorption process. The negative ΔG values indicate that the adsorption process is thermodynamically feasible at studied temperatures. It is clear that the entropy values increase as follows: MMB > RB. It means that the adsorption of CV^+ onto MMB sample gives a less-order system than that onto RB sample. The reorientation or restructuring of water around CV^+/bentonite complex is

Table 3
Langmuir and Freundlich isotherm parameters for the adsorption of CV^+ onto bentonite samples

Sample	Langmuir isotherm constants			Freundlich isotherm constants			D-R isotherm constants		
	q_m (mmol/g)	K_L (L/mmol)	R^2	n	K_f (mmol $^{(1-1/n)}$ $L^{1/n}$/g))	R^2	q_m (mmol/g)	E (kJ/mol)	R^2
RB	0.32	1.61	0.959	3.58	0.83	0.982	0.42	11.47	0.962
MMB	1.12	5.59	0.969	14.92	1.11	0.985	1.12	19.55	0.845

Table 4
Thermodynamic parameters for the adsorption of CV^+ onto bentonite samples

Sample	ΔH (kJ/mol)	ΔS (J/(mol K))	ΔG (kJ/mol)				R^2
			295.15 K	300.15 K	305.15 K	309.15 K	
RB	117.41	41.50	−5.07	−7.15	−9.22	−10.88	0.991
MMB	21.19	98.34	−7.84	−8.33	−8.82	−9.22	0.999

Contact time 4 h, C_0 = 2.5 mmol/L, initial pH 6.0, m = 2 g/L.

very unfavorable in terms of entropy, since CV^+/bentonite complex disturbs the existing water structure and imposes a new and more disordered structure on the surrounding water molecules. The positive values of ΔS suggest the randomness at the solid–solution interface increases during the adsorption process, since the CV^+ species adsorbed leads to a decrease in the number of the water molecules. Furthermore, values of $T_{av}\Delta S$ can be calculated from the experimental data where T_{av} represents the average values of the range of temperature used for adsorption studies. It is found that $\Delta H < T_{av}\Delta S$ for the both type of the bentonites (the values are ΔH (117.41) > $T_{av}\Delta S$ (125.58) and ΔH (21.19) < $T_{av}\Delta S$ (29.74) for RB and MMB, respectively). This means, although contribution of ΔH is not negligible, the influence of entropies are more remarkable. The different values of the thermodynamic parameters for the bentonite samples implicate a non-uniform thermodynamic process taking place during the bentonite–CV^+ interaction.

3.6. Adsorption kinetic

The adsorption data for the uptake of CV^+ vs. contact time at different initial concentrations ranging from 0.6 to 2.0 mmol/g is presented in Figs. 5 and 6. It is also clear from these figures that the equilibrium time was achieved after 200 min for RB and 25 min MMB sample, respectively. The high rate of CV^+ adsorption onto MMB may be attributed to the modified surface properties of bentonite. As given in Table 1, the BET surface area of MMB is markedly higher than that of RB, indicating that the time required to reach equilibrium is directly correlative with the surface area. Surface area measurement for MMB was marked on anhydrous sample, the hydrated sample is expected to be much greater surface area than the measured value because the oxide swells in aqueous phase [38].

Tables 5 and 6 list the results of the rate constant studies for different initial dye concentrations by the pseudo-first-order and pseudo-second-order models at 295.15 K. It is seen that the correlation coefficient of pseudo-first-order kinetic are lower than in the case of pseudo-second-order kinetic model. This finding shows that kinetics of dye adsorption by bentonites are better described by pseudo-second-order kinetic model rather than pseudo-first-order model. For the pseudo-second-order model in Tables 5 and 6, the rate constants for the both type of bentonites generally decreased with the increase of the initial dye concentration.

As given in Tables 5 and 6, the rate constant of CV^+ uptake was found to decrease from 5.59×10^{-2} to 2.63×10^{-2} g/(mmol min) for RB. At lower concentrations, CV^+ ions present in the adsorption medium could interact with the binding sites, hence higher rate constant results. At higher concentrations, because of the satura-

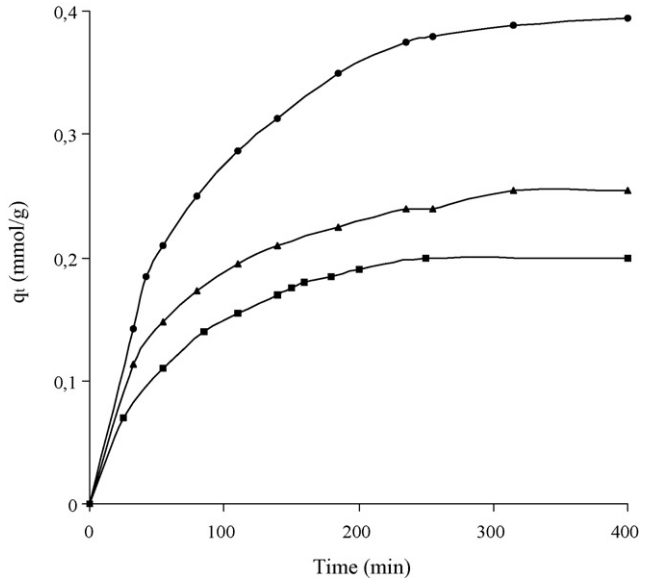

Fig. 5. Plots of adsorbed CV^+ amount vs. time onto the RB sample at different initial CV^+ concentrations, 0.6 mmol/g, circles; 1.2 mmol/g, triangles; 2.0 mmol/g, squares. T = 295.15 K, initial pH 6.0, and m = 2 g/L.

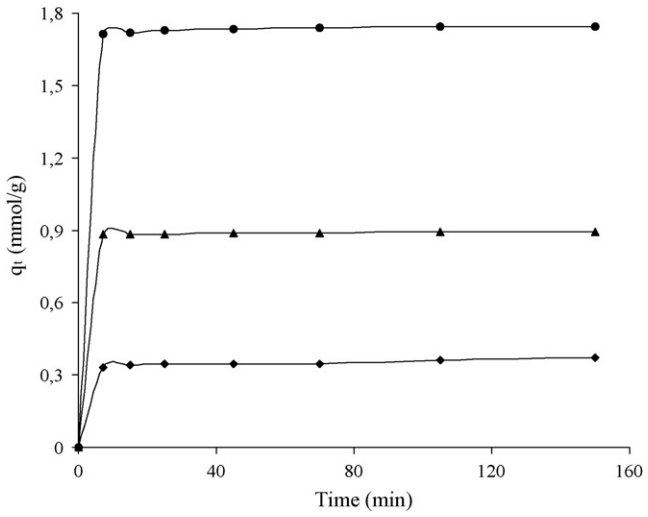

Fig. 6. Plots of adsorbed CV^+ amount vs. time onto the MMB sample at different initial CV^+ concentrations, 0.6 mmol/g, circles; 1.2 mmol/g, triangles; 2.0 mmol/g, squares. T = 295.15 K, initial pH 6.0, and m = 2 g/L.

Table 5
Kinetic parameters for the adsorption of CV^+ onto RB sample at different initial dye concentrations

C_0 (mmol/g)	Pseudo-first-order model		Pseudo-second-order model		
	$R_1{}^2$	k_1 ($\times 10^2$ min^{-1})	$R_2{}^2$	$q_{e,2}$ (mmol/g)	$k_2 \times 10^2$ (g/(mmol min))
0.6	0.997	1.16	0.999	0.25	5.59
1.2	0.970	1.09	0.999	0.29	5.53
2.0	0.997	1.12	0.998	0.49	2.63

Table 6
Kinetic parameters for the adsorption of CV^+ onto MMB sample at different initial dye concentrations

C_0 (mmol/g)	Pseudo-first-order model		Pseudo-second-order model		
	R_1^2	$k_1(\times 10^2\ min^{-1})$	R_2^2	$q_{e,2}$ (mmol/g)	$k_2 \times 10^2$ (g/(mmol min))
0.6	0.894	0.04	0.999	0.38	66.72
1.2	0.925	0.54	0.999	0.90	154.35
2.0	0.929	0.51	0.999	1.76	81.38

tion of the adsorption sites, the rate constant of dye adsorption onto the bentonites shows a decreasing trend. This is due to after the initial stage of adsorption, the remaining vacant surface sites are difficult to be occupied due to repulsive forces between the CV^+ molecules on the bentonite surface. It is observed in Table 6 that when the CV^+ initial concentration increases from 0.6 to 1.2 mmol/g, the rate constant, k_2, increases from 66.72×10^{-2} to 154.35×10^{-2} mmol/(g min), but further increase in initial concentration to 2.0 mmol/g causes the reverse trend and decrease to 81.38 mmol/(g min). Similiar observations were reported in the literature [39–41].

3.7. Adsorption mechanism

Although the kinetic studies help in identifying the adsorption process, the determination of the adsorption mechanism is important for design purposes. There is a possibility that the transport of the CV^+ from the solution into the pores of the bentonites is rate controlling. Hence, the data were further processed for testing the role of diffusion in the adsorption process. Figs. 7 and 8 show a plot of q_t vs. $t^{1/2}$ for the present system. The plot of q_t against $t^{1/2}$ may present a multi-linearity correlation, which indicates that two steps occur during adsorption process. For the adsorption process onto RB, the first linear portions in Fig. 7 could be due to intraparticle diffusion effects. The slopes of these linear portions can be defined as a rate parameter and characteristic of the rate of adsorption in the region where intraparticle diffusion is occurring. Initially, within a short-time period, it is postulated that the dye was transported to the external surface of the RB through film diffusion and its rate have been very fast. After saturation of the surface, the dye molecule entered into the RB particle by intraparticle diffusion through pore and interior surface diffusion until equilibrium is attained which is represented by the second straight lines in Fig. 7. As given in Table 7, it is obvious that values of k_i increase from 11.02×10^{-3} to 18.09×10^{-3} when the initial CV^+ concentration is increased from 0.6 to 2.0 mmol/g. It is also observed that the value of the intercept increases from 2.64×10^{-2} to 7.79×10^{-2}, which indicates that the thickness of the boundary layer increases significantly with increase of initial dye concentration. Several previous investigations have reported a similiar type of pattern [37,42]. As shown in Fig. 8, the shape of plots for MMB is different from Fig. 7. It seems that the shape of plots is nearly the same for studied

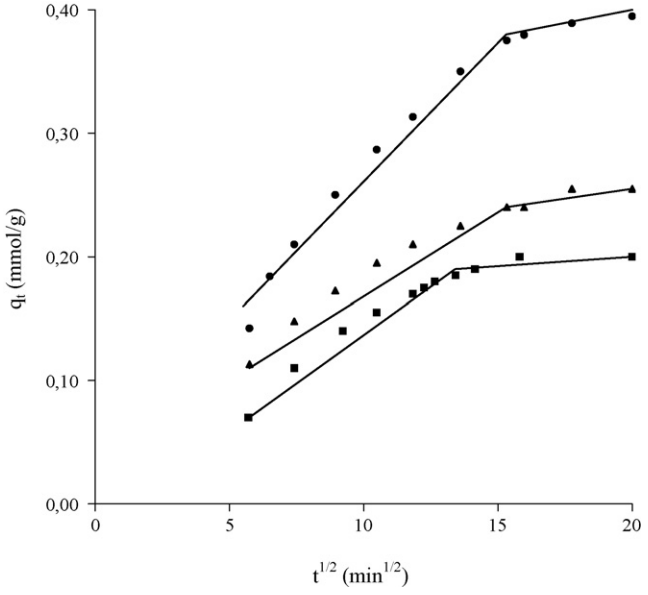

Fig. 7. Amount of dye adsorbed vs. $t^{1/2}$ for intraparticle diffusion of CV^+ by RB sample at different initial CV^+ concentrations, 0.6 mmol/g, squares; 1.2 mmol/g, triangles; 2.0 mmol/g, circles. T = 295.15 K, initial pH 6.0, and m = 2 g/L.

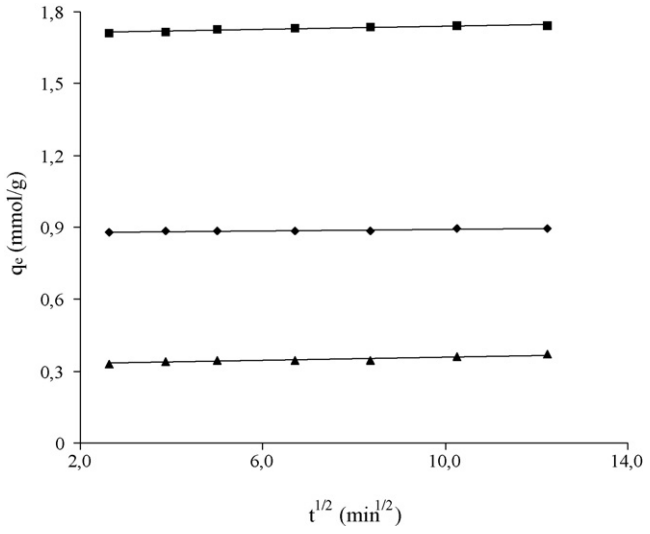

Fig. 8. Amount of dye adsorbed vs. $t^{1/2}$ for intraparticle diffusion of CV^+ by MMB sample at different initial CV^+ concentrations, 0.6 mmol/g, squares; 1.2 mmol/g, triangles; 2.0 mmol/g, circles. T = 295.15 K, initial pH 6.0, and m = 2 g/L.

Table 7
Intraparticle diffusion constants for the adsorption of CV^+ onto MMB sample at different initial dye concentrations

C_o (mmol/g)	RB			MMB		
	R_i^2	$k_i \times 10^3$ (mmol/(g min$^{1/2}$))	$c \times 10^2$ (mmol/(g min$^{1/2}$))	R_i^2	$k_i \times 10^3$ (mmol/(g min$^{1/2}$))	$c \times 10^2$ (mmol/(g min$^{1/2}$))
0.6	0.898	11.02	2.64	0.962	3.84	32.22
1.2	0.922	12.94	7.89	0.943	1.57	87.55
2.0	0.925	18.09	7.79	0.968	3.47	170.65

Table 8
Adsorption results of basic dyes from the literature by various adsorbents

Adsorbent	Dye	Adsorption capacity (mg/g)	Reference
Bentonite	MG	≈7.7	[28]
Calcium alginate beads	BB	≈58	[40]
Activated carbon prepared from rattan sawdust	MB	≈294	[43]
Activated carbon produced from New Zealand coal	MB	580	[44]
Oil palm fibre activated carbon	MB	≈278	[45]
Silkworm pupa	BB 41	555	[46]
Jute fiber carbon	CV^+	≈28	[47]
Saw dust	CV^+	341	[48]
Apricot stone activated carbon	AB FGRL	≈182	[49]
Sepiolite	AB FGRL	≈156	[49]
Fly ash	AB FGRL	≈129	[49]
Activated carbon prepared from rattan sawdust	MB	≈294	[50]
Pomelo peel	MB	≈345	[51]
RB	CV^+	0.32 mmol/g = 131 mg/g	In this study
MMB	CV^+	1.12 mmol/g = 457 mg/g	In this study

MG: malachite green; MB: methylene blue; BB: basic black, AB FGRL: Astrazon Blue FGRL.

concentration values. When the concentration of the dye solution increased from 0.6 to 2.0 mmol/g, the intraparticle diffusion rate constants were not changed, indicating that the intraparticle diffusion is not rate-limiting step, but other kinetic models control the rate of adsorption.

3.8. Comparison of dye removal with different adsorbents reported in literature

The adsorption capacities of the adsorbents for the removal of CV^+ have been compared with those of other adsorbents reported in literature and the values of adsorption capacities have been presented in Table 8. The values reported in the form of monolayer adsorption capacity. The experimental data of the present investigation are comparable with the reported values [28,40,43–51]. The maximum adsorption capacity of dye for MMB sample is approximately 3.5 times higher than that for RB. From this table, it is appeared that the surface properties of raw bentonite could be improved upon modification of manganese oxide.

4. Conclusions

The amount of dye adsorbed was found to vary with initial CV^+ concentration, contact time and temperature. MMB has higher adsorptive capacity for CV^+ than RB which can be attributed to the effect of pH_{PZC} and the physcial characteristics of both adsorbents. When the equilibrium solution pH exceeds the pH_{PZC}, an enhancement in the adsorptive capacities was observed. The Langmuir equilibrium constant K_L for the MMB value (5.59) was much higher than that for the RB (1.61). Therefore, MMB not only had a higher adsorption capacity than that of RB, but it also contained sites with higher binding energy for CV^+. The adsorption intensity given by the Freundlich coefficient (n) is higher than 1 (the values for the RB and MMB are 3.58 and 14.92, respectively) for the bentonite samples. It was found that the kinetics of the adsorption of CV^+ onto bentonite samples at different initial concentrations was best described by the pseudo-second-order model. Based on the results, it was concluded that MMB had a significant potential for removing basic dye from wastewater using adsorption method.

References

[1] G. Mckay, S.J. Allen, J.F. Porter, J. Colloid Interf. Sci. 280 (2004) 322–333.
[2] P.F. Luckham, S. Rossi, Adv. Colloid Interf. Sci. 82 (1999) 43–92.
[3] S.S. Tahir, R. Naseem, Sep. Purif. Technol. 53 (2007) 312–321.
[4] E. Eren, B. Afsin, J. Hazard. Mater. 151 (2008) 682–691.
[5] Z. Rawajfih, N. Nsour, J. Colloid Interf. Sci. 298 (2006) 39–49.
[6] S. Andini, R. Cioffi, F. Montagnaro, F. Pisciotta, L. Santoro, Appl. Clay Sci. 31 (2006) 126–133.
[7] M. Akçay, G. Akçay, J. Hazard. Mater. 113 (2004) 189–193.
[8] F. Ayari, E. Srasra, M. Trabelsi-Ayadi, Desalination 206 (2007) 499–506.
[9] A. Demirbas, A. Sari, O. Isildak, J. Hazard. Mater. 135 (2006) 226–231.
[10] M. Bacquet, B. Martel, M. Morcellet, K.I. Benabadji, K. Medjahed, A. Mansri, A.-H. Meniai, M. Bencheikh Lehocine, Mater. Lett. 58 (2004) 455–459.
[11] T. Asselman, G. Garnier, Colloids Surf. A 168 (2000) 175–182.
[12] E. Bojemueller, A. Nennemann, G. Lagaly, Appl. Clay Sci. 18 (2001) 277–284.
[13] J. Bors, S. Dultz, B. Riebe, Appl. Clay Sci. 16 (2000) 1–13.
[14] Q.-Y. Yue, Q. Li, B.-Y. Gao, Y. Wang, Sep. Purif. Technol. 54 (2007) 279–290.
[15] E. Eren, B. Afsin, Dyes Pigments 76 (2008) 220–225.
[16] M. Al-Ghouti, M.A.M. Khraisheh, M.N.M. Ahmad, S. Allen, J. Colloid Interf. Sci. 287 (2005) 6–13.
[17] M.A. Al-Ghouti, M.A.M. Khraisheh, M.N. Ahmad, S.J. Allen, J. Hazard. Mater. 146 (2007) 316–327.
[18] M.M. Mohamed, I. Othman, R.M. Mohamed, J. Photochem. Photobiol. A: Chem. 191 (2007) 153–161.
[19] E. Eren, J. Hazard. Mater. 159 (2008) 235–244.
[20] E. Eren, B. Afsin, Y. Onal, J. Hazard. Mater. 161 (2009) 677–685.
[21] R. Dohrmann, Appl. Clay Sci. 34 (2006) 31–37.
[22] K. Fuda, S. Narita, J. Ceram. Soc. Jpn. 112 (2004) 717–723, Special issue.
[23] R.W. Grimshaw, The Chemistry and Physics of Clays and Allied Ceramic Materials, 4th ed., Ernest Benn Lmt, London, 1971, 968–978.
[24] I. Langmuir, J. Am. Soc. 40 (1918) 1361–1403.
[25] H. Freundlich, Z. Phys. Chem. 57 (1906) 385–470.
[26] A.R. Cestari, E.F.S. Vieira, G.S. Vieira, L.E. Almeida, J. Colloid Interf. Sci. 309 (2007) 402–411.
[27] C.A. Başar, J. Hazard. Mater. 135 (2006) 232–241.
[28] S.S. Tahir, N. Rauf, Chemosphere 63 (2006) 1842–1848.
[29] S. Lagergren, About the theory of so-called adsorption of soluble substances, Kungliga Svenska Vetenskapsakademiens Handlingar 24 (4) (1898) 1–39.
[30] Y.S. Ho, G. McKay, J. Environ. Sci. Health A 34 (1999) 1179–1204.
[31] W.J. Weber, J.C. Morris, J. Sanit. Eng. Div. Am. Soc. Civil Eng. 89 (1963) 31–60.
[32] G. Szöllösi, A. Mastalir, M. Bartok, React. Kinet. Catal. Lett. 74 (2001) 241–249.
[33] D. Dermatas, M.S. Dadachov, Appl. Clay Sci. 23 (2003) 245–255.
[34] T. Boonfueng, L. Axe, Y. Xu, J. Colloid Interf. Sci. 281 (2005) 80–92.
[35] P.F. Luckham, S. Rossi, Advan. Colloid Interf. Sci. 82 (1999) 43–92.
[36] Y.G. Mishael, G. Rytwo, S. Nir, M. Crespin, F. Annabi-Bergaya, H. Van Damme, J. Colloid Interf. Sci. 209 (1999) 123–128.
[37] M. Alkan, S. Çelikçapa, Ö. Demirbaş, M. Doğan, Dyes Pigments 65 (2005) 251–259.
[38] J. Kärger, D.M. Ruthven, Diffusion in Zeolites and Other Microporous Solids, Wiley, New York, 1992 (referenced from [24]).
[39] M.I. El-Khaiary, J Hazard. Mater. 147 (2007) 28–36.
[40] R. Aravindhan, N.N. Fathima, J.R. Rao, B.U. Nair, Colloids Surf. A 299 (2007) 232–238.
[41] M.H. Isa, L.S. Lang, F.A.H. Asaari, H.A. Aziz, N.A. Ramli, J.P.A. Dhas, Dyes Pigments 74 (2007) 446–453.
[42] I.D. Mall, V.C. Srivastava, N.K. Agarwal, J. Hazard. Mater. 143 (2007) 386–395.
[43] B.H. Hameed, A.L. Ahmad, K.N.A. Latiff, Dyes Pigments 75 (2007) 143–149.
[44] E.N. El Qada, S.J. Allen, G.M. Walker, Chem. Eng. J. 135 (2008) 174–184.

[45] I.A.W. Tan, B.H. Hameed, A.L. Ahmad, Chem. Eng. J. 127 (2007) 111–119.
[46] B. Noroozi, G.A. Sorial, H. Bahrami, M. Arami, J. Hazard. Mater. 139 (2007) 167–174.
[47] K. Porkodi, K. Vasanth Kumar, J. Hazard. Mater. 143 (2007) 311–327.
[48] S. Chakraborty, S. De, S. DasGupta, J.K. Basu, Chemosphere 58 (2005) 1079–1086.
[49] B. Karagozoglu, M. Tasdemir, E. Demirbas, M. Kobya, J. Hazard. Mater. 147 (2007) 297–306.
[50] B.H. Hameed, A.L. Ahmad, K.N.A. Latiff, Dyes Pigments. 75 (2007) 143–149.
[51] B.H. Hameed, D.K. Mahmoud, A.L. Ahmad, Colloids Surf. A 316 (2008) 78–84.